LABORATOIRE
Jean Perrin

Master Physics of Complex Systems

M2 Internship Report – Academic Year 2020-2021

Optogenetic perturbations to unveil brain-scale functional organization in zebrafish larva

---

Author :
Alexandre NAULEAU

Supervisors :
Georges DEBRÉGEAS
Volker BORMUTH

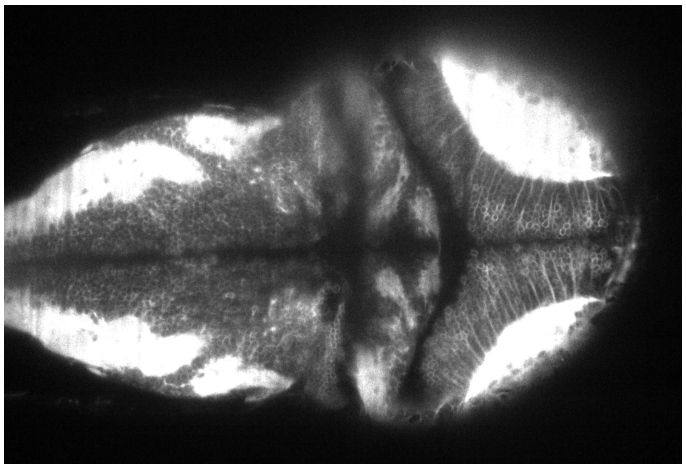

Laboratoire Jean Perrin
-
UNIVERSITÉ PIERRE ET MARIE CURIE

Acknowledgements

I would like to thank all the members of the team who gave me precious advice during these three last months: **Guillaume Le Goc**, **Geoffrey Migault**, **Sharbatanu Chatterjee**, **Natalia Belén Beiza Canelo**, **Julie Lafaye**, **Thomas Panier**, **Mattéo Dommanget-Kott**, **Hippolyte Moulle**, and **Sophia Karpenko**.

I would like also to acknowledge **Volker Bormuth** and **Georges Debrégeas** for their supervision.

Summary

In spite of their apparent stochasticity, neuronal circuits display a highly structured spontaneous activity even in the absence of sensory stimulation. Large-scale recordings have shown that neuronal network dynamics is characterized by the coordinated activity of so-called cell assemblies, which can be identified using dimensionality reduction techniques. This complex activity is well modelled by attractor states associated to specific behavioral patterns. Understanding the computational origin of these states and the mechanisms underlying spontaneous transitions between them is a longstanding major issue in systems neuroscience. As part of my M2 internship project, I developed an experimental approach in order to study evoked neuronal activity in the vertebrate brain. I used a recently developed platform in my laboratory enabling both local perturbation of neuronal activity with one-photon optogenetics and whole-brain imaging with light-sheet microscopy. These methods allowed me to induce brain-scale perturbations in the zebrafish larva brain, a widely used vertebrate model organism in neuroscience, and concurrently record the activity of almost all the 100,000 neurons constituting its brain. Perturbing brain activity is of major importance for testing causal interactions in neuronal networks, understand the contribution of small neuronal populations and establish a functional connectivity between different regions. I developped a stimulation protocol testing the effect of different stimulation intensities and durations over the whole brain activity. Brain-wide responses were specific of the stimulation region. The computation of correlation between the activities of different regions enabled me to establish a brain-scale functional connectivity map. Besides allowing an unprecedented exploration of the zebrafish brain dynamics at all spatial scales, these results will allow to directly connect neurophysiological circuit properties with a recently probabilistic graphical model developed in collaboration with my laboratory, called compositional Restricted Boltzmann Machines, aiming at capturing neuronal activity statistics in a physiologically interpretable way. This *in silico* model will allow to predict perturbations of neuronal activity at whole brain scale and will sharply contrast to currently used blackbox-like machine learning techniques.

Contents

Acronyms

cRBM compositional Restricted Boltzmann Machines

dpf days post fertilization

LSM Light Sheet Microscopy

GECIs Genetically Encoded Calcium Indicators

GFP Green Fluorescent Protein

RBM Restricted Boltzmann Machines

ROI Region of interest

Introduction

Neural networks are intrinsically stochastic, displaying *in vivo* variability both in spontaneous and evoked neuronal activity [1]. In systems neuroscience, neurons are thought to constitute information processing units able to process inputs and produce adequate outputs given environmental and internal conditions [2]. Electrophysiological recordings revealed that neuronal network dynamics is characterized by the coordinated activity of cortical assemblies of excitatory and inhibitory neurons [3]. This complex dynamics is highly structured and supposed to have major functional roles. For instance, sensory spontaneous activity has been shown to capture the statistics of natural stimuli in the environment [4]. The structure of spontaneous activity of neuronal assemblies can be identified through dimensionality reduction techniques aiming at describing high-dimensional neural systems with as few variables as possible[5]. A wide range of theoretical models has already been introduced in order to analyze neuronal recordings in a low dimension space but these models are not easily interpretable in neurophysiological terms [6].

Generative probabilistic graphical models like Restricted Boltzmann Machines (RBM) naturally provide this quality. Indeed, it has been shown that these network models allow the inference of detailed functional connectivity between neurons with a possible connection to behavioral activity [7]. The model architecture is a two-layer network that maps neurons to cell assemblies and naturally allows the study of high-dimensional data because higher-order interactions are explicitly represented in the network so that functionally correlated ensembles of neurons naturally emerge. Moreover, instead of deterministic approaches of dimensionality reduction such as Principal Component Analysis, RBM are probabilistic so that they are fully adapted to evaluate the likelihood of a given neuronal pattern activity. This is of major importance since it allows to generate artificial data from inferred probability distributions. Thus, a well trained RBM model will be able to generate neuronal activity characterized by the same statistics than recorded spontaneous neuronal activity.

Perturbing brain activity is of major importance for testing causal interactions in neuronal networks, understand the contribution of small neuronal populations and establish a functional connectivity between different regions. [8] Here, we investigate the brain-scale functional organization in zebrafish larva using light-induced activation of spatially-defined neuronal populations in order to directly interrogate neural circuit activity. In order to implement this technique, we use one-photon optogenetic activation and simultaneous assessment of activated neuronal circuits by whole-brain *in vivo* calcium imaging with light-sheet microscopy.

1.1 The zebrafish larva, a model organism

The zebrafish (*Danio rerio*) is a freshwater fish originating from South Asia. Widely used as an aquarium fish, it was introduced as a vertebrate model organism in the scientific community in the seventies, first in genetics and developmental biology and more recently in neuroscience. Indeed, it combines many advantages. The larva has the property of being almost transparent which makes

it very easy to record neuronal activity *via* non invasive methods like fluorescence microscopy techniques. Moreover, the adult fish has a small size (approximately 3-4 cm) and a short life cycle, reaching adulthood at three months. In addition, the larval brain is small (1 mm x 0.5 mm x 0.5 mm), containing around 100,000 neurons although the fish has a rich behavioural repertoire. It is currently the only vertebrate system accessible to functional imaging from whole-brain to cellular level.

1.2 Optogenetics and calcium imaging

Optogenetics is a neuroscience technique, at the interface of optics and genetics, allowing to control the activity of neurons using light, with a single-cell spatial precision and a millisecond-scale temporal precision [9]. These neurons have been genetically modified in order to express a light-sensitive membrane protein. The most known family is channelrhodopsins whose first discovered members - Channelrhodopsin-1 (ChR1) and Channelrhodopsin-2 (ChR2) - have been originally isolated from the single cell green alga *Chlamydomonas reinhardtii*. ChR2 is a transmembrane protein containing a photo-sensitive chromophore whose absorption spectrum is peaked at 480 nm. When this chromophore is excited by a photon with a close wavelength, its conformation is modified and induces the opening of a pore into the neuron membrane, leading to a flow of cations into the neuron and then to its depolarization. For my experiments, I used a fish line expressing the recently discovered high-photocurrent channelrhodopsin CoChR (extracted from the alga *Chloromonas oogama*) [10].

Genetically encoded calcium indicators (GECIs) are well suited to record neuronal activity over periods of milliseconds to months. They can monitor the concentration of free calcium in neurons. Currently, Green fluorescent protein (GFP) based fluorophores are widely used for *in vivo* electrophysiology as it is a non-invasive method to record neuronal activity. GCaMP indicators are a family of calcium indicators resulting from the assembly of an enhanced GFP, a calmodulin (**cal**cium-**modul**ated prote**in**) which is a ubiquitous protein, able to associate with intra-cellular calcium ions, and a peptide M13. The fixation of a Ca^{2+} ion on the calmodulin triggers a conformational change of the peptide M13 which in turn leads to a change in the conformation of the eGFP and increases its quantum efficiency (*i.e.* the fraction of photons absorbed versus emitted). GCaMPs have successively been modified in order to improve the amplitude of their fluorescence intensity and therefore their signal-to-noise ratio. For my experiments, I used the calcium indicator called jRGECO1b, which is derived from the mApple red fluorescent protein and has a sensitivity comparable to GCaMP6 [11]. We made this choice because the GCaMP excitation spectrum overlaps with channelrhodopsin-2's, which makes it complicated to use simultaneously green GECIs and optogenetics. Red-shifted GECIs provide several advantages compared to the green ones: in addition to allowing a parallel use of optogenetic tools, they reduce photodomage (in particular photobleaching) because they limit light absorption in tissue and scattering [11].

1.3 Towards a probabilistic graphical model of whole brain activity

My laboratory, in collaboration with the Statistical physics group of Rémi Monasson (ENS Paris), developed a new probabilistic graphical model has been developped called compositional Restricted Boltzmann Machines (cRBM). cRBM is a maximum-entropy model, meaning that it makes the fewest *a priori* assumptions, defining the maximally random model reproducing the data statistics. In RBM, the connections between neurons and so-called hidden units reflect data statistics. The model architecture is a two-layer network that maps neurons to cell assemblies and naturally allows the study of high-dimensional data because higher-order interactions are explicitly represented in the network so that functionally correlated ensembles of neurons naturally emerge. Moreover, instead of deterministic approaches of dimensionality reduction such as Principal Component Analysis, RBM are probabilistic so that they are fully adapted to evaluate the likelihood of a given neuronal pattern activity. This is of major importance since it allows to generate artificial data by Monte Carlo sampling from inferred probability distributions. Thus, a well trained RBM model will be able to generate neuronal activity characterized by the same statistics than recorded spontaneous neuronal activity. All in all, these RBM models provide two main advantages: introduce higher-order correlations between neurons in order to study the emerging population dynamics and identify collective modes, i.e. neuronal groups with correlated or synchronized activity. Recently, an extension of RBM called compositional RBM (cRBM) has been introduced and brings the RBM into the so-called compositional phase, ensuring that neuronal activity can be decomposed in assemblies that co-activate in a time-dependent way to compose the brain-wide neuronal activity.

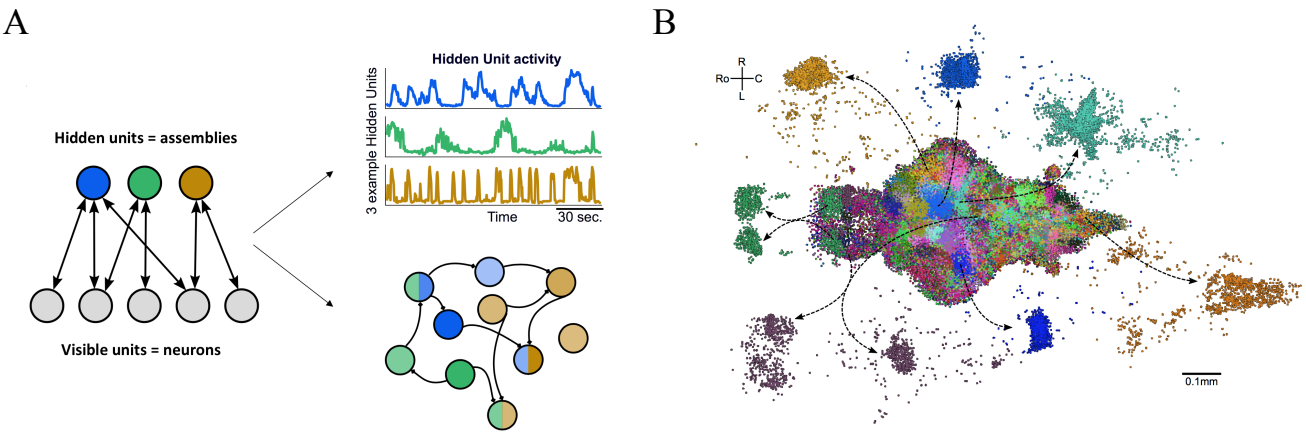

Figure 1: compositional Restricted Boltzmann Machines (cRBM), a probabilistic graphical model capturing neuronal activity statistics. **A.** Bipartite graph constituting the cRBM. The visible units, representing the physical neurons, are linked to the so-called hidden units representing cell assemblies. Once the model has been trained, neural data statistics are reproduced by the connection weights in the model. It allows to infer the activity cell assemblies and the whole functional connectivity between them. **B.** Map of cell assemblies localization in the larval zebrafish brain. Each cell assembly can be mapped to a particular anatomical region. All cell assemblies span the entire brain. (illustrations adapted from [12]).

The energy of the model is given by:

$$E(\mathbf{v},\mathbf{h}) = -\sum_i g_i v_i + \sum_\mu U_\mu\left(h_\mu\right) - \sum_{i,\mu} w_{i,\mu} v_i h_\mu \tag{1.1}$$

where the so-called visible units v_i represent the physical neurons, the hidden units h_μ are latent variables corresponding to cell assemblies (*i.e.* groups of neurons which tend to be co-activated). The fields g_i and potentials U_μ control the activity level of the visible units and the marginal distribution of the hidden units respectively. $w_{i,\mu}$ represents the weight between the neuron i and the hidden unit and the joint probability distribution to be in a configuration $(\mathbf{v},\mathbf{h})$ is given by the so-called Boltzmann distribution:

$$P(\mathbf{v},\mathbf{h}) = \frac{1}{Z}\exp\left(-E(\mathbf{v},\mathbf{h})\right) \tag{1.2}$$

1.4 M2 internship project

The aim of my internship is to interrogate neuronal circuits at the scale of the whole brain in zebrafish larva. To do so, we used a one-photon optogenetic system coupled to volumetric functional imaging using *in vivo* calcium imaging with a light sheet microscope. To conduct this project, we used fish lines expressing the channelrodopsin CoChR coupled to the enhanced GFP and the calcium indicator jRGECO1b in the cytoplasm of almost all neurons (*Tg(elavl3:CoChR-eGFP);Tg(elavl3:jRGECO1b))*. This was a total exploratory approach since no one had tried to do optogenetics experiments on these fish lines before in the laboratory. Expression patterns of GFP and jRGECO1b are respectively represented in Figures 3A and 3B.

The eGFP coupled to the channelrhodopsin allows to visualize the expression pattern of the latter whereas the jRGECO1b is the calcium indicator. When a neuron is activated, there is a rapid increase of the intracellular calcium concentration. Then, the calcium indicator can fix some free Ca^{2+} ions which induces a change of its conformation and an increase of its fluorescence intensity. Thus, the recorded fluorescence intensity is indirectly linked to neuronal activity.

For the experiments, we used a whole brain volumetric imaging through light sheet microscopy (LSM). Light sheet microscopy is a fluorescence microscopy technique allowing to illuminate a single plane in a sample, which allows to drastically reduce photobleaching (*i.e.* the photochemical alteration of a fluorophore leading to a loss of fluorescence) and increases the speed of scanning the sample unlike a confocal microscope where the sample is illuminated point by point. Optical sectioning is obtained because the lightsheet is around 3-5 µm thick, i.e. comparable to the size of an individual neuron. For experiments, the zebrafish larva was tethered in low-melting-point agarose. It is a gel containing mostly water and typically 2% of agarose which makes the compound solid at room temperature. It is porous enough to allow the fish to live for days in this restrained condition because larval zebrafish of a few days post fertilization (dpf) can breathe by diffusion of oxygen through the skin. Then, in order to prepare the fish for imaging, it is aspired into a glass capillary (see Figure 2A) which is inserted in a specific holder put under the observation objective.

Given that agar is 98% composed of water, it has a refractive index very similar to water and thus produces minimal optical aberrations. Using this technique, we can study spontaneous neuronal activity or expose the animal to specific sensory stimuli to see how the brain reacts and try to understand how, where and when the stimulus is perceived and integrated.

We used Light Sheet calcium imaging to record the activity of around 50,000 neurons during 2 minutes for each larva, at a rate of 2 brain scans per second. The principle of LSM is illustrated in Figure 2B. The sample is illuminated from one side at a single plane level. This illumination excites fluorophores contained in this xy plane. All neurons located in this plane can thus be imaged rapidly in the z direction, allowing for high frame rate imaging. The light sheet is then scanned rapidly in the z-direction to image multiple layers and build volumetric images of the sample. Here, each brain scan consists of 25 layers separated by 10 µm. These images are then analyzed by first segmenting individual neurons, then by computing the relative change in fluorescence intensity $\Delta F/F$ = (F(t) - baseline)/(baseline - background) for every neuron (see Material and methods for more details).

In a first time, we tried to characterize the properties of the optogenetic stimulation, especially to quantify the optical sectioning of the system, a crucial parameter for targeted local perturbations. We also characterized the fluorescence intensity response of our transgenic zebrafish lines for different stimulation intensities. Then, we tried to gain insight into the effects of optogenetic perturbation to whole brain activity.

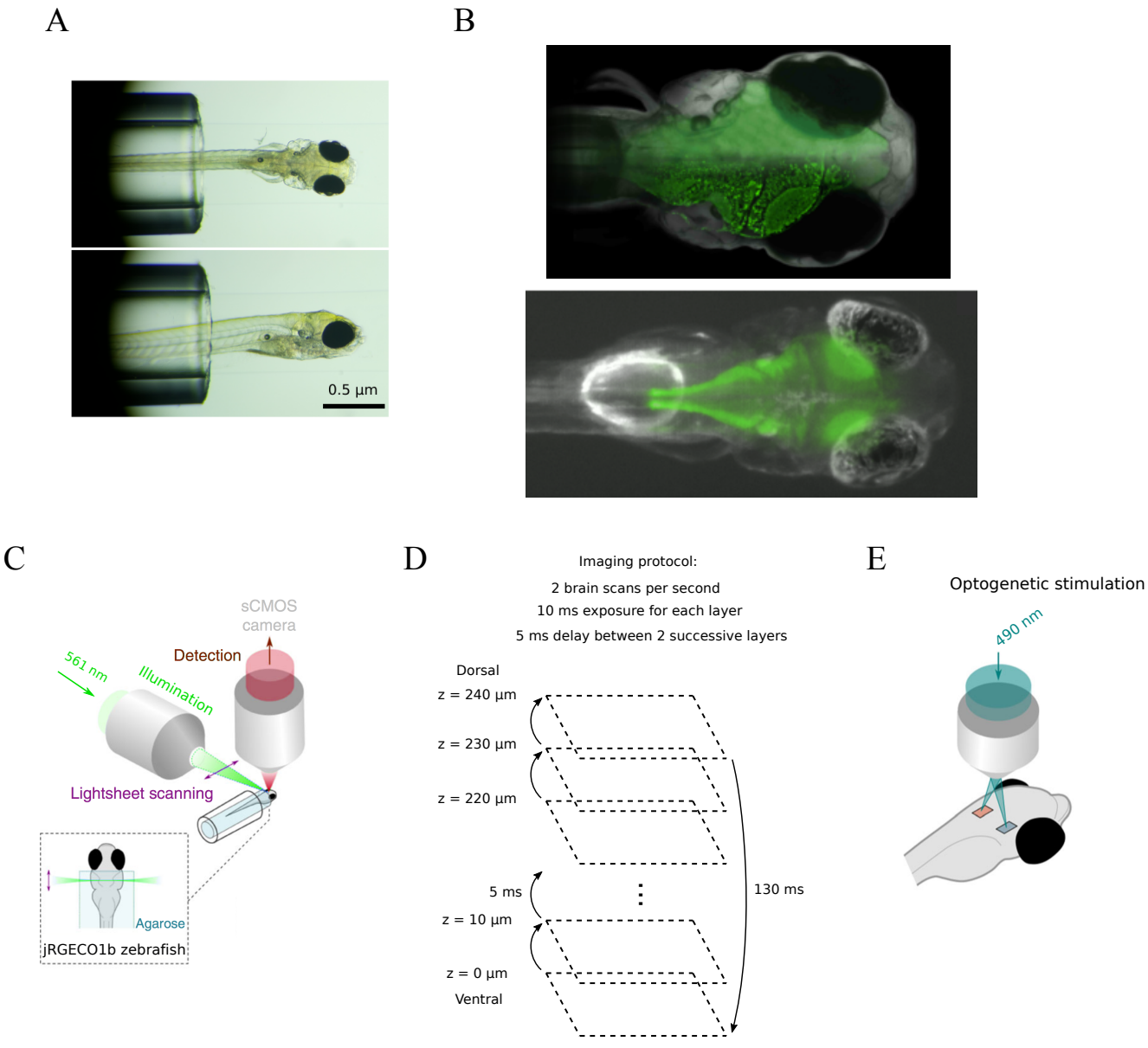

Figure 2: Experimental setup and imaging protocol. **A.** Top and side views of a 5 dpf zebrafish larva mounted in a glass capillary. The zebrafish is maintained into agarose and slightly moved out of the capillary before imaging its brain. **B.** GCaMP fluorescence of the brain in a larval zebrafish. On the top image, the bottom side is recorded with two-photon scanning microscope whoch allows a good z-sectioning and the other side with bright field fluorescence microscopy (illustration obtained from Engertlab). On the bottom image, GCaMP green fluorescence recorded with a light-sheet microscope (illustration from laboratoire Jean Perrin). **C.** Simplified representation of a Light Sheet Microscope. The illumination light, in green, comes from the side of the fish and excites the calcium indicators in a single plane, allowing a good optical sectioning. Emitted photons, in red, are detected on top of the fish by a sCMOS camera. **D.** Imaging protocol for volumetric imaging. 25 layers of the brain are imaged along the vertical axis, from the ventral to the dorsal part of the fish. Two successive layers are separated by 10 µm and temporal acquisition parameters are such that 2 brain scans are performed each second. **E.** Simplified representation of an optogenetic stimulation. The stimulation region is predefined by drawing at hand a mask on a given z-layer (see examples of masks in supplementary Figure 18).

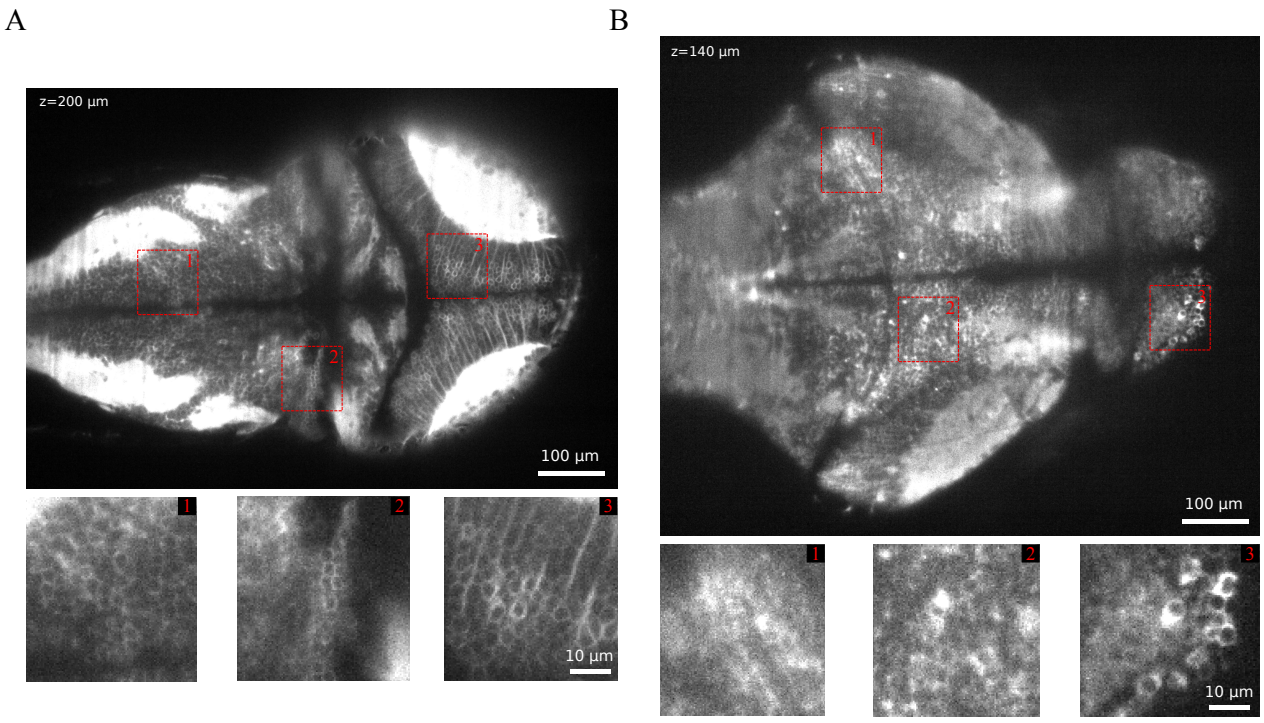

Figure 3: Expression patterns of the elavl3:CoChR-eGFP ; elavl3:jRGECO1b line. **A.** GFP fluorescence of a 5 dpf transgenic zebrafish larva and enlarged views of three regions marked by red boxes. The green fluorescent protein is coupled to the channelrhodopsin CoChR and thus reveals its expression pattern. **B.** RGECO fluorescence of a 5 dpf transgenic zebrafish larva and enlarged views of three regions marked by red boxes.

Characterization of the optogenetic stimulation

2.1 Spatial resolution and optical sectioning

As confirmed by Figure 4A, the one-photon system we used for the stimulation does not have z resolution. Indeed, the light stimulation is not focused on a specific layer but forms in the stimulated region a light column illuminating all the layers from the ventral part to the dorsal part of the brain. The side view of fluorescence intensity profiles, represented in Figure 4B shows that the maximum intensity of fluorescence slowly decays in the layers before and after the stimulation layer represented in red. The 3D plots represented in Figures 4C and 4D shows how the intensity profiles evolve with the stimulation intensity. We can see for example that the maximum fluorescence intensity change from around 700 a.u. to around 1150 a.u. when the intensity of the stimulation is multiplied by 10.

2.2 Effect of varying stimulation intensities on fluorescence activity

We studied the effect of different stimulation intensities on recorded fluorescence activity, stimulating the larval zebrafish brain 2s every 10s for a total duration of 120s (see Materials and Methods) In response to an optogenetic stimulation, a high increase of the relative change in fluorescence is recorded (a typical trace is shown in Figure 5A). In order to determine an optimal stimulation intensity for our optogenetic stimulation, we varied the stimulation intensity from 10% to 100 % of LED intensity. The resulting averaged traces are shown in Figure 5B. For each trace, we can distinguish the same characteristic events: (1) first a silent period before the stimulation then (2) a quasi instantaneous rise of ΔF/F, (3) a slower increase, (4) a quasi-instantaneous decrease of ΔF/F and then (5) a return to the activity level before the stimulation. We quantified the rise time of ΔF/F during the stimulation period, for each stimulation intensity. Obtained results are represented in Figure 6A. The mean rise time continuously decreases from 0.79 ± 0.07 s at 10% stimulation intensity to 0.50 ± 0.02 s at 100% stimulation intensity. As a consequence, at least two different timescales can be distinguished. The first one is a very short timescale associated to illumination light and responsible for the rapid rise (2) and decrease (4) of fluorescence activity. The second one is a slower timescale (4) associated to the calcium indicator RGECO whose typical decay time is of the order of the second at room temperature [11], as confirmed by the mean decay times we estimated in Figure 6.

In order to show whether the slow rise of ΔF/F in stage (3) was only due to the opening kinetics of channelrhodopsin, we tried to do the same optogenetic stimulation with a control fish not expressing channelrhodopsin (cf supplementary Figure 13). We observed the same slow rise of ΔF/F but with a slower kinetics, the mean rise time was equal to 0.37 ± 0.02 s. The presence of this slow rise of relative fluorescence change, even in the absence of channelrhodopsin, can probably be explained by photoactivation of the jRGECO1b. Indeed, it has been shown that the derivatives

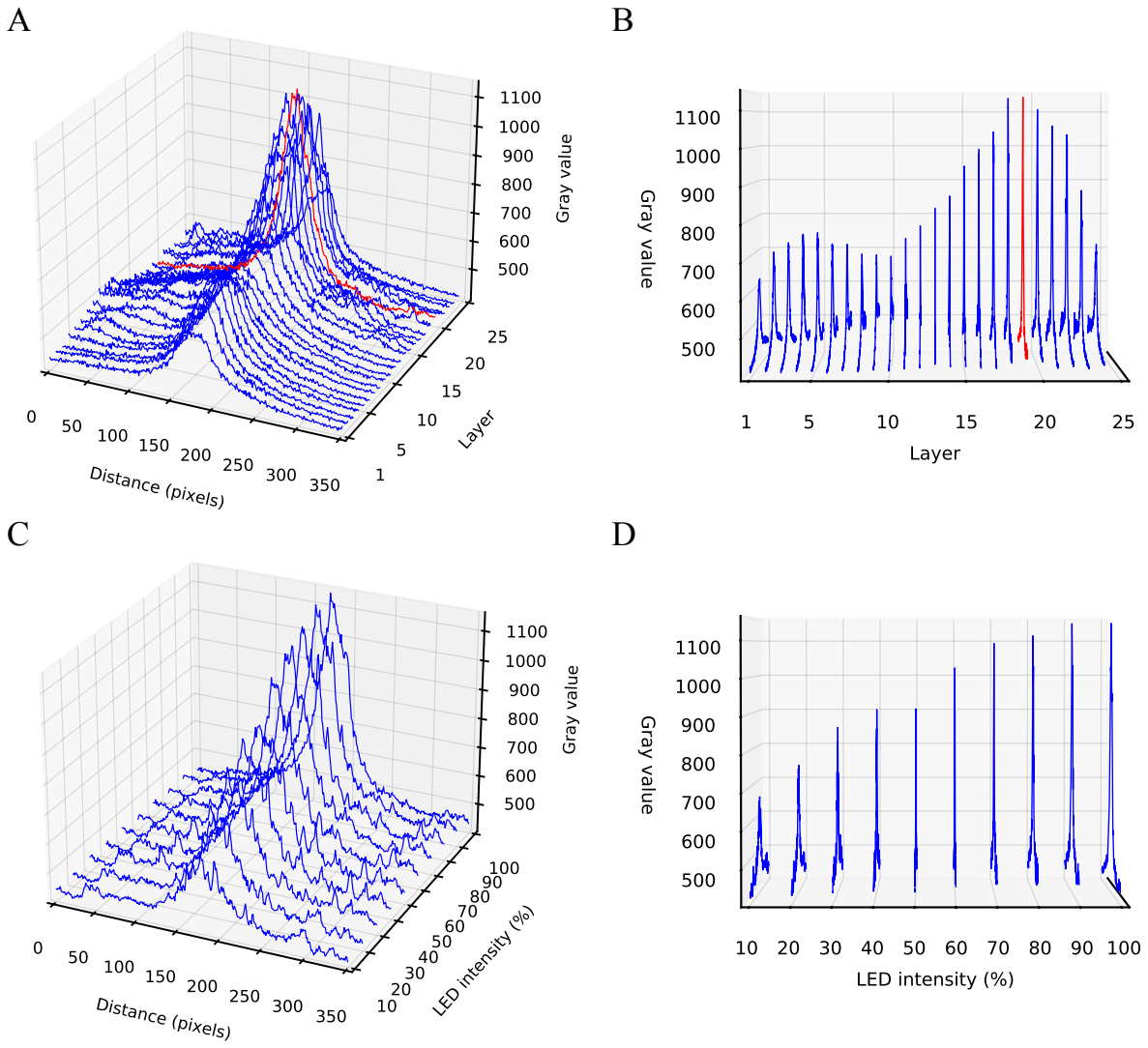

Figure 4: jRGECO1b fluorescence intensity profiles and lack of optical sectioning of the one-photon optogenetic stimulation. **A.** Intensity profiles of red calcium indicator jRGECO1b for the first 24 layers of the brain of a 5 dpf zebrafish larva. The z-positions of the layers are defined according to the imaging protocol represented in Figure 2C. The red profile corresponds to the stimulation layer. Gray value represents the fluorescence intensity in arbitrary units (see Materials and Methods for more details). **B.** Side view of the same plot **C.** Fluorescence intensity profiles in the stimulation layer for 10 different stimulation intensities (from 10% to 100% of LED intensity). **D.** Side view of the same plot.

of RGECO1 (jRGECO1a and jRGECO1b) exhibit photoswitching in response to blue light [11].

We also studied the amplitudes of rapid increase and decrease respectively occurring at stimulation onset and offset, as a function of LED intensity (see Figure 5C). These amplitudes were well fitted by a power law $y = ax^b$. We obtained a=0.045 $\pm$ 0.003 and b=0.732 $\pm$ 0.015 for the amplitudes at stimulation onset, a=0.063 $\pm$ 0.005 and b=0.746 $\pm$ 0.020 for the amplitudes at stimulation offset. Amplitudes at stimulation offset were always higher than the ones at stimulation

onset. We interpreted it saying that the amplitude at stimulation offset included two components: the fluorescence signal due to illumination onset and the fluorescence signal due to the activity of jRGECO1b.

Finally, the decay amplitude observed just after the stimulation, corresponding to stage (5), was quantified (see Figure 5D). It evolves from 0.17 ± 0.02 at 10% stimulation intensity to 0.22 ± 0.01 at 100% stimulation intensity and seems to saturate for stimulation intensities between 20% and 30%. We also compared it to the one estimated for the control fish. We found, at 100% stimulation intensity and for 2s optogenetic stimulations, that the average decay amplitude was about two times higher in presence of channelrhodopsin compared to the control (respectively 0.22 ± 0.01 vs 0.09 ± 0.02) confirming that a part of the $\Delta F/F$ signal observed after the stimulation is due to the presence of channelrhodopsin and therefore neuronal activity. In order to demonstrate that some part of the decaying signal is not coming from the illumination light itself, we did another control. We illuminated agarose containing a red fluorescent dye (4-di-2asp, see supplementary Figure 14). There was no detectable decay amplitude just after an optogenetic stimulation, confirming that the LED illumination light does not contribute to the observed post-stimulation decaying amplitude in transgenic zebrafish.

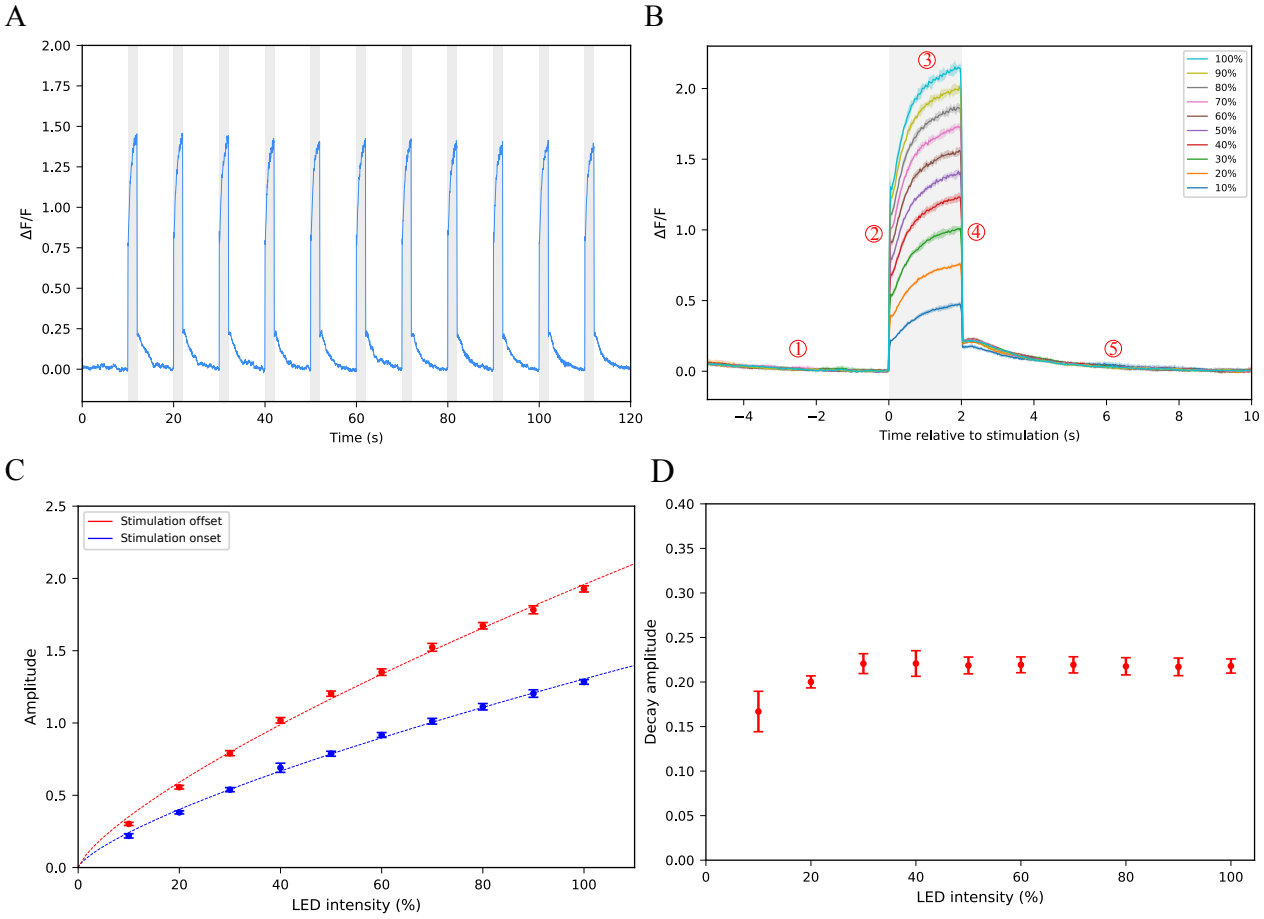

Figure 5: Effect of varying stimulation intensities on fluorescence activity. **A.** Typical trace of relative change of fluorescence for a stimulation at 50% of LED intensity. Gray shaded regions represent stimulation periods. **B.** Relative change of fluorescence activity for 10 different stimulation intensities (from 10% to 100% of LED intensity). For each stimulation intensity, the thick line represents the mean value and shaded regions the standard deviation. The gray shaded region is the stimulation period. The red circled numbers represent the 5 characteristic stages described in the main text. **C.** Amplitudes of relative change of fluorescence at stimulation onset and offset as a function of stimulation intensity. Dots represent mean values over 10 trials and error bars indicate standard deviation. **D.** Decay amplitude as a function of stimulation intensity. Dots represent mean values over 10 trials and error bars indicate standard deviation.

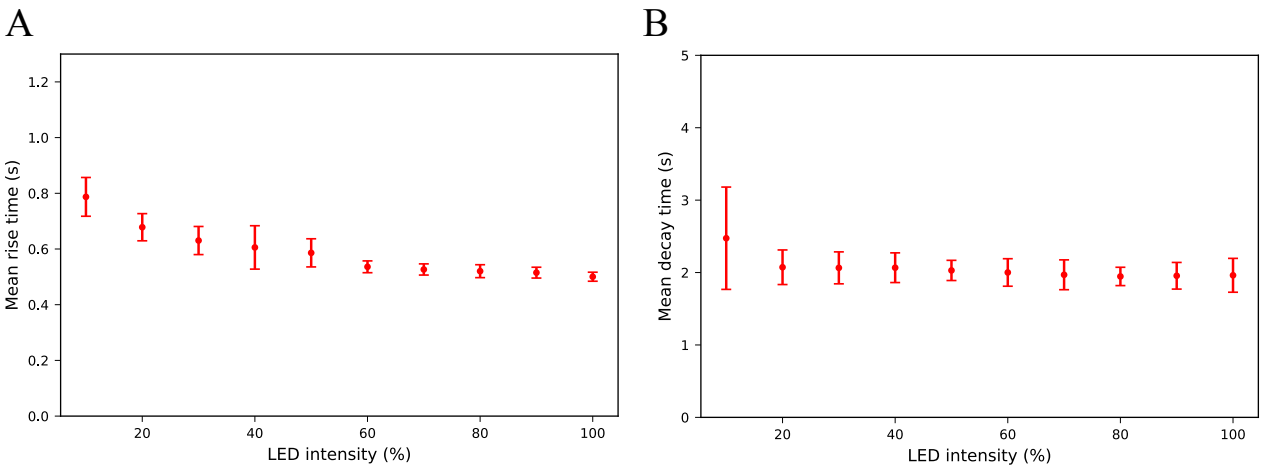

Figure 6: Mean rise and decay times of fluorescence activity as a function of stimulation intensity. **A.** Mean rise time of fluorescence activity as a function of stimulation intensity (corresponds to stage (3) in Figure 5B). **B.** Mean decay time of fluorescence activity as a function of stimulation intensity (corresponds to stage (5) in Figure 5B).

Towards a brain scale functional connectivity map

3.1 A specific brain-wide response triggered by optogenetic stimulation

In order to characterize the influence of the stimulated region over the brain activity, we tried to stimulate the brain in two different regions defined on the same layer (cf stimulation masks of Figure 7).

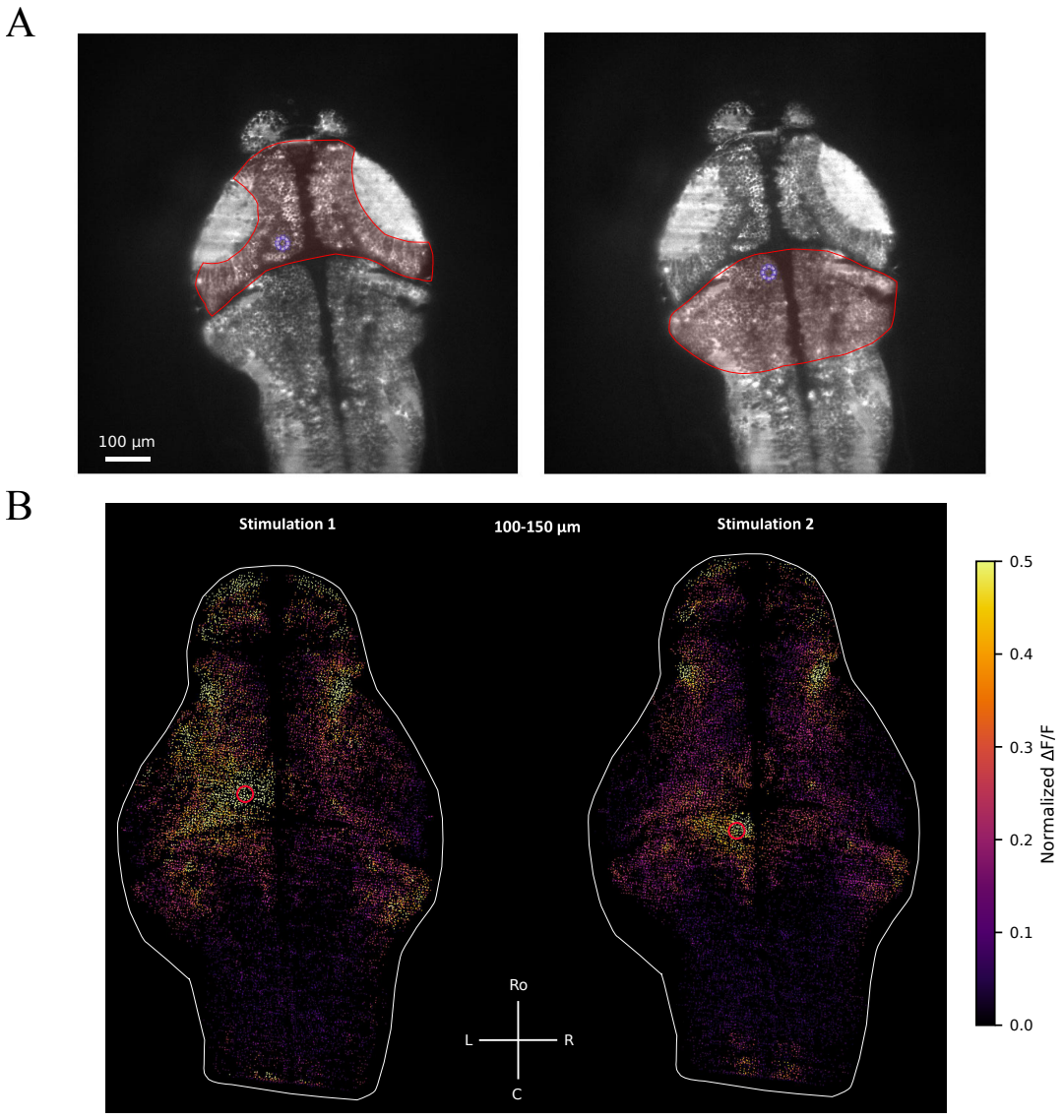

Figure 7: A brain-wide perturbation of neuronal activity specific to the optogenetically targeted site. **A.** Stimulation sites are defined by the drawn mask (small blue circle). Stimulation 1 has been drawn in the optic tectum (red shaded region on the left image) whereas stimulation 2 (right) is located in the cerebellum (red shaded region on the right image). **B.** Activation pattern in the layers between 100 and 150 µm from ventral part of the fish during the optogenetic stimulation for each stimulation region. The brain response is specific to the stimulated region. White line represents brain contours. Ro: Rostral, C: Caudal, L: Left, R: Right

The optogenetic stimulation elicited a brain-wide specific response. We can see in Figure 7B that the hindbrain has a very low activity for both stimulations. The extent of the activation is larger for the stimulation in the optic tectum compared to the one in the cerebellum. The pallium is also more activated in the first stimulation compared to the second one.

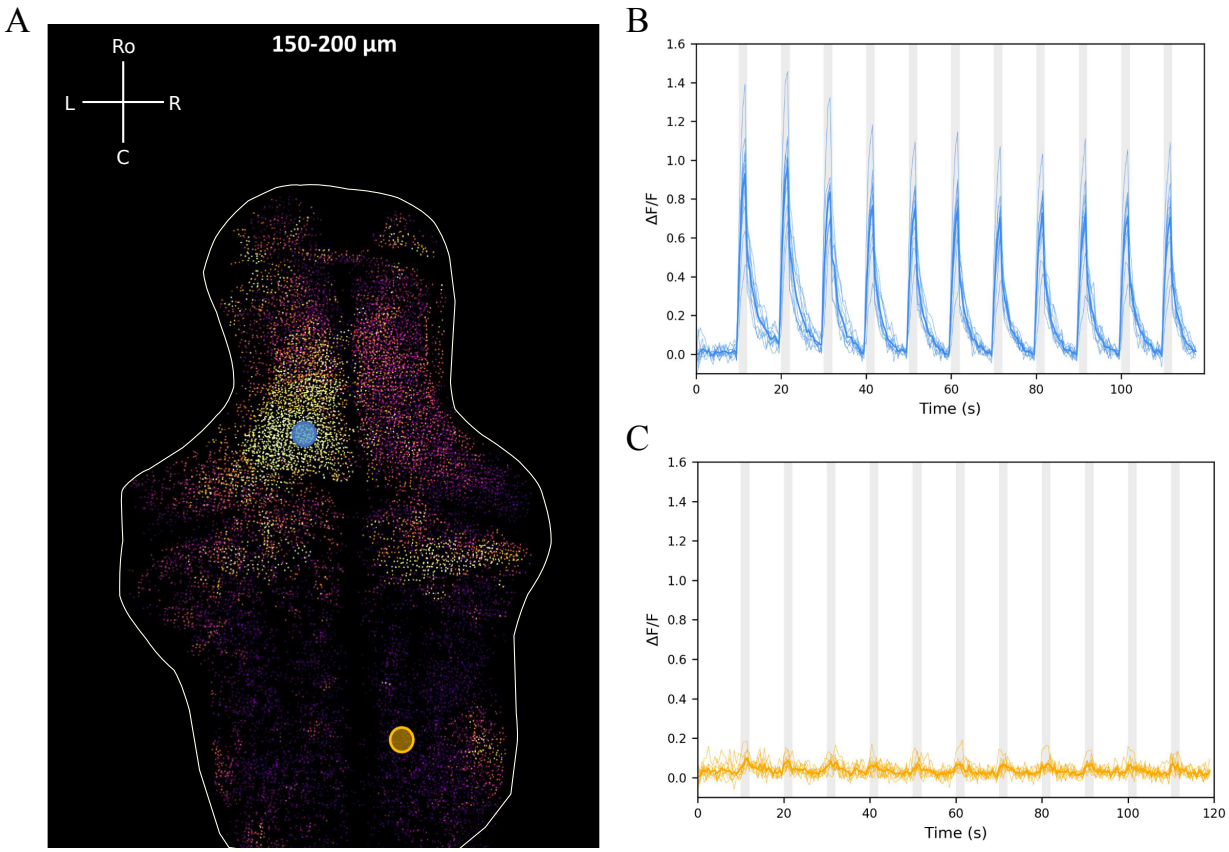

Figure 8: A brain-wide perturbation of neuronal activity in response to a stimulation in the optic tectum. **A.** Top view of the neurons included in the layers between 150 and 200 µm from ventral part of the fish during the optogenetic stimulation. White line represents brain contours. Colors represent normalized ΔF/F activity (same colorbar as Figure 7). **B.** Relative change of fluorescence in the stimulated region (blue circle on panel A). Thick line represent the mean ΔF/F and shaded areas the standard deviation. Gray shaded regions correspond to the stimulation periods. **B.** Relative change of fluorescence in an other region (hindbrain, orange circle on panel A). Thick line represent the mean ΔF/F and shaded areas the standard deviation. Gray shaded regions correspond to the stimulation periods. Ro: Rostral, C: Caudal, L: Left, R: Right

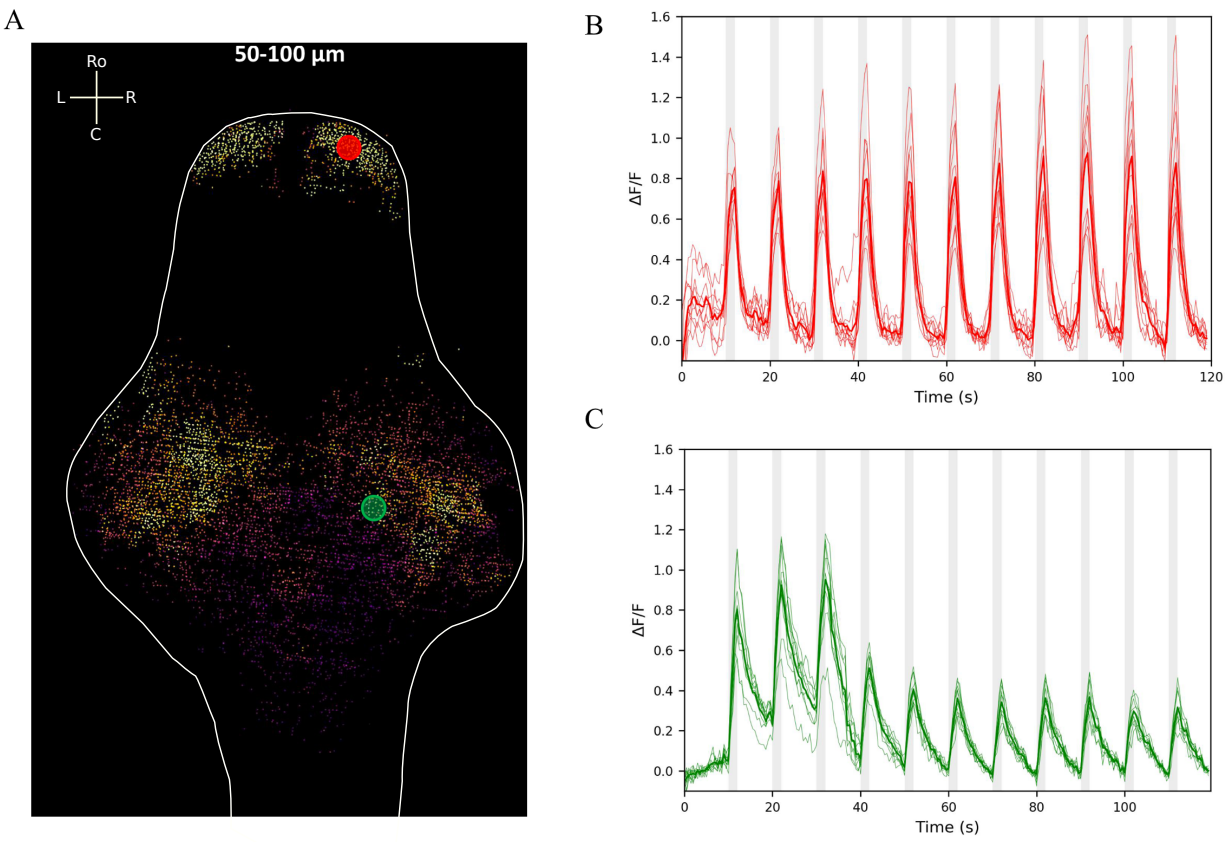

Figure 9: A brain-wide perturbation of neuronal activity in response to a stimulation in the optic tectum. **A.** Top view of the neurons included in the layers between 50 and 100 µm from ventral part of the fish during the optogenetic stimulation. White line represents brain contours. Colors represent normalized ΔF/F activity (same colorbar as Figure 7). **B.** Relative change of fluorescence in the pallium (red circle on panel A). Thick line represent the mean ΔF/F and shaded areas the standard deviation. Gray shaded regions correspond to the stimulation periods. **B.** Relative change of fluorescence in an other region (midbrain, green circle on panel A). Thick line represent the mean ΔF/F and shaded areas the standard deviation. Gray shaded regions correspond to the stimulation periods. Ro: Rostral, C: Caudal, L: Left, R: Right

As we can see in Figures 8 and 9, the optogenetic stimulation induced in a particular region of the brain (here the optic tectum) triggers a whole brain response. In Figure 8 are represented the temporal evolution of the relative fluorescence intensity in two different regions: in the stimulation region in blue (optic tectum) and in the hindbrain in orange. In Figure 9 is represented the mean ΔF/F trace in the pallium in red and in the midbrain in green. Responses are quantitatively different in all these regions: in the stimulated region (blue, Figure 8), the mean ΔF/F trace is high during stimulation periods and then decays slowly until the beginning of the next stimulation. It seems that there is a decay of the peak intensity with a slower timescale. In the hindbrain (orange, Figure 8), the ΔF/F trace is slightly modified during each stimulation (ΔF/F peaks at around 0.15) but the activity always remains very close to the one before the first stimulation. In the pallium (red, Figure 9), the mean ΔF/F trace has peaks of intensities slightly lower compared to those in the stimulated

region and their intensities increase over time. In the midbrain (green, Figure 9), the mean activity is high during the first three stimulations and then drops until the last stimulation. These results illustrate the diversity and complexity of whole brain evoked activity in response to locally targeted optogenetic perturbation.

3.2 A brain-wide functional connectivity map

In order to compute Pearson correlation matrices between different brain regions, we discretized the whole brain volume into voxels such that the size of each voxel is the same for each dimension. The mean number of neurons in each voxel was about 200 and the total number of non empty voxels was 337. A top view of the voxelization is shown in Figure 10A. Then, we computed the mean $\Delta F/F$ in each voxel only taking into account periods of no stimulation. Indeed, as we have seen before, the stimulation seems to largely activate the majority of voxels (probably because the stimulation intensity is too high) and taking into account these stimulation periods would bias the Pearson correlations. We obtained the correlation matrix represented in Figure 10B. It seems that, even without taking into account stimulation periods, the activities of a large number of voxels are highly correlated (> 0.8) which results in the presence of red blocks in the correlation matrix.

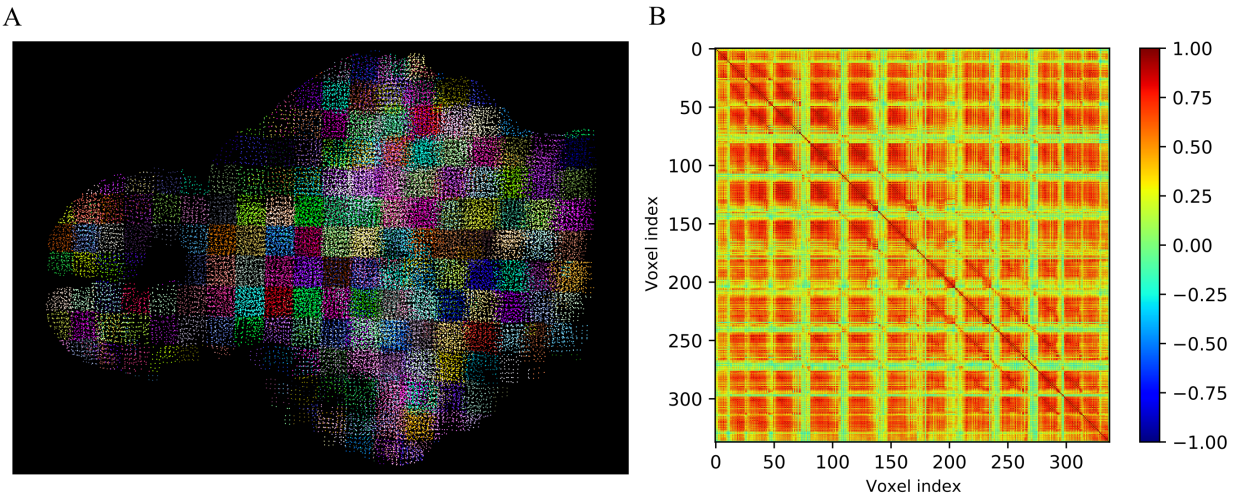

Figure 10: Pearson correlation matrix and brain-wide activity in response to optogenetic stimulation. **A.** Top view of the zebrafish brain after the voxelization process. Each dot is a neuron. A random color has been assigned to each voxel for visualization. **B.** Pearson correlation matrix between activities of voxels during off-stimulation periods.

Then, we tried to stimulate the optic tectum and the hindbrain (see stimulation masks in Figure 18) for different durations, from 20 ms to 4s (see Material and methods) and at maximum intensity (to be sure to have a neuronal response, even at very low stimulation durations). As we see in Figure 11, for 2s of stimulation, almost all voxels are highly active during each stimulation period. For 200 ms of stimulation, a majority of voxels are always active during stimulation periods, but

with a lower normalized ΔF/F than before. Finally, for 20 ms stimulation, the normalized ΔF/F is very weak for most voxels. A comparison between these activities in the optic tectum and in the cerebellum is illustrated in supplementary Figure 17. When the stimulation is located in the cerebellum, voxel activities are globally less active than when the optic tectum is stimulated.

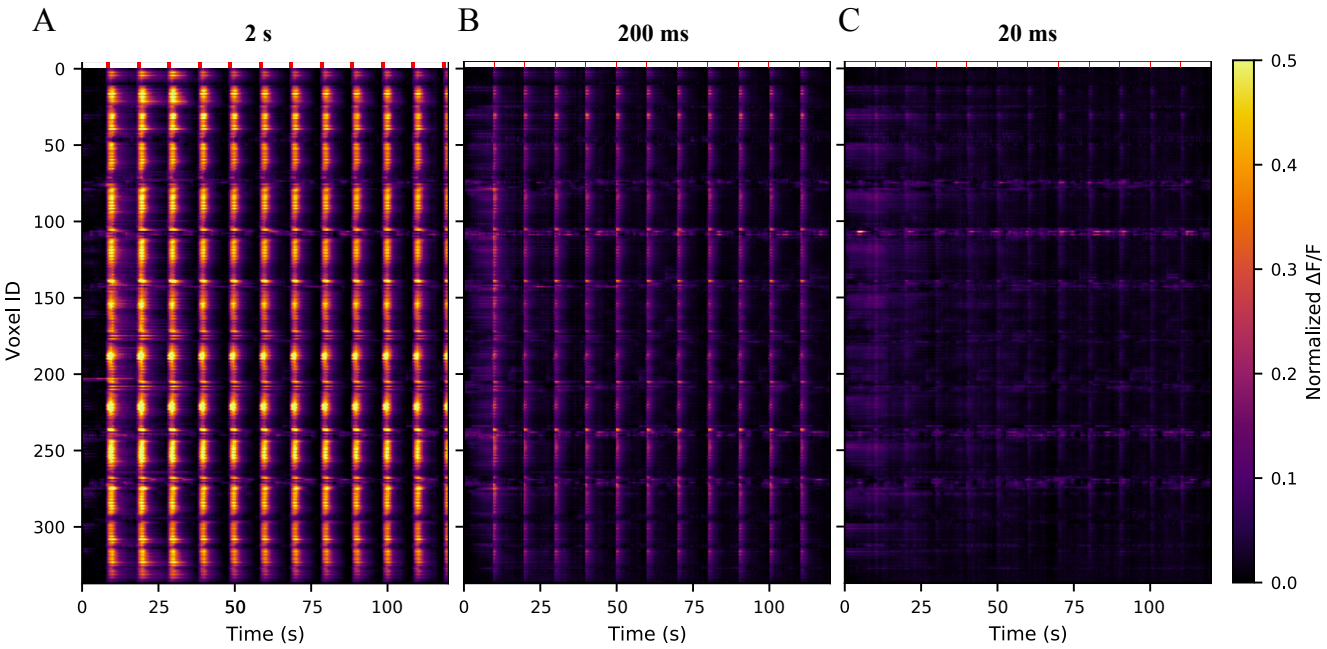

Figure 11: Brain-wide activity in response to an optogenetic stimulation in the optic tectum for three different stimulation times. Red top ticks represent stimulation durations. **A.** Normalized ΔF/F activity for 2 s of stimulation at 100% of stimulation intensity. **B.** Normalized ΔF/F activity for 200 ms of stimulation at 100% of stimulation intensity. **C.** Normalized ΔF/F activity for 20 ms of stimulation at 100% of stimulation intensity.

Conclusions and Perspectives

In the framework of this M2 project, we obtained preliminary results showing that we can study the whole brain response of zebrafish larva and interrogate specific neuronal populations by locally perturbing the neuronal activity. The experimental setup we used allowed me to concurrently perform local perturbations of neuronal activity and whole brain *in vivo* calcium imaging in order to better understand the functional organization of the zebrafish brain.

From the preliminary results obtained, we demonstrated that a part of the relative change of fluorescence we observed after an optogenetic stimulation was due to the presence of channelrhodopsin and then related to neuronal activity. However, at maximum stimulation intensity, about half of the observed response was potentially due to a photoswitching effect exhibited by the calcium indicator when illuminated with blue light [11]. This problem could be solved by changing the illumination system for the optogenetic stimulation using a two-photon device. Indeed the excitation light for a two-photon system is in the infrared (typically higher than 800 nm), a wavelength at which the photoswitching behavior of jRGECO1b is not observed [11]. Another issue we encountered was the absence of optical sectioning for the stimulation. Indeed, as confirmed by spatial profiles of optogenetic stimulations along all layers defined in the brain, the one-photon optogenetic system we used does not have z resolution. Once again, the use of a two-photon system will solve this problem. My laboratory will shortly acquire a two-photon 3D holographic optogenetic system, which will allow to selectively stimulate a precisely defined 3D population in the brain and reproduce some experiments we made during my internship.

Finally, in the scope of my PhD project, all these preliminary results will enable me to develop a multidisciplinary approach in order to unravel the fundamental principles underlying spontaneous neuronal activity. The developed hybrid approach, both experimental and theoretical, will allow me to measure spontaneous and evoked neuronal activity at all spatial scales using whole-brain calcium imaging and produce an efficient and predictive statistical model of this activity with an interpretable architecture tailored to the zebrafish system. Finally, the effects of local perturbation of neuronal activity through targeted optogenetic stimulations will be recorded and then compared with the statistical model predictions of brain state distributions and transitions. The possibility of automating these experiments will make it possible to rapidly establish complete response maps in a reduced time scale and offer the potentiality to obtain a mesoscale functional connectivity map of the larval zebrafish brain. All in all, the developed functional model will allow to identify neuronal attractor states, associated with specific behavioral patterns, as well as the mechanisms underlying the spontaneous transitions between these states.

Materials and Methods

5.1 Transgenic zebrafish larvae

The transgenic zebrafish larvae we used were coming from a crossing between *casper* background females expressing channelrhodopsin in the cytoplasm under the control of the nearly pan-neuronal promoter elavl3 *Tg(elavl3:CoChR-eGFP)* and *nacre* background males expressing jRGECO1b in the cytoplasm *Tg(elavl3:jRGECO1b)*. Fish lines were provided by Misha B. Ahrens of Janelia (Howard Hughes Medical Institute, USA). Larvae were reared in Petri dishes in E3 solution on a 14/10 hour light/dark cycle at 28°C. Petri dishes were washed by hand every day. All imaged fish were between 5 and 7 dpf. Fish were screened before 5 dpf in orderFish were paralyzed before imaging by an exposure of 1 min 30 s to 1 mg/mL α-bungarotoxin (Thermofisher Scientific) in E3 medium. They were subsequently transferred to pure E3 medium and we waited about 30 min to check for normal heart beating and absence of motor activity.

5.2 Processing of calcium activity data

Image pre-processing, segmentation of individual neurons and computation of relative change of fluorescence over time (ΔF/F) were performed offline using MATLAB, according to the workflow previously developed in the laboratory [13]. XY drifts were corrected by registering each image of the stack with respect to the first image by extracting the displacement vector that provided the maximum correlation. Segmentation of individual neurons were performed using a Watershed algorithm. Next, we extracted the fluorescence time signals F(t) for selected regions of interest (ROIs) by evaluating the mean intensity across the pixels within each ROI, in each motion-corrected image. We estimated the relative variations of the fluorescence intensity, ΔF/F, with respect to the baseline signal as ΔF/F = (F(t) - baseline)/(baseline - background) [13]. The background was estimated from the average intensity of pixels outside the brain and the baseline fluorescence signal was estimated for each ROI by a running 10^{th} percentile estimation of the fluorescence time signal in a sliding window of 50 s. The latter calculation was performed with the "runnquantile" function, which is part of the "caTools" CRAN R-package (https://CRAN.R-project.org/ package=caTools). We called this function directly from MATLAB.

5.3 Light sheet imaging

For light sheet imaging, we used a green LASER at 561 nm wavelength at a power of 35 mW. We acquired 1,024 × 1,024 pixel images, over 25 z locations spaced 10 µm apart, at a 2 Hz volumetric-imaging rate. The acquisition settings for the light-sheet imaging data are shown in Figure 2B. Each layer was exposed during 10 ms, the delay between two successive layers was 5 ms and the long delay to go from the most dorsal layer to the most ventral one was 130 ms. For each imaged

layer, the temporal resolution of the recording was 500 ms (one acquisition of a whole layer every 500 ms).

For single layer acquisitions, we acquired images with the same resolution and also used 10 ms exposure so that the temporal resolution of the recording was 30 ms.

Emitted photons were collected by a detection objective after passing through a bandpass Texas Red filter centered in 630 nm ($\pm$ 69 nm).

5.4 Optogenetic stimulation

Optogenetic stimulations were performed using a Cool-LED pE-4000 illumination system at a wavelength of 490 nm. The stimulation region was defined by drawing a mask on the computer associated to the set up *via* a Matlab interface, controlling a Digital Micromirror Device (DMD) allowing to produce a localized pattern of illumination, by controlling the position of each micromirror. The stimulation durations were directly entered in a file setting up the stimulation parameters. In all figures, reported stimulation intensities in the report are indicated as a percent of the maximum stimulation intensity at this wavelength which is 87 mW. Then the stimulation intensities 10%, 20%, 30%, 40%, 50%, 60%, 70%, 80%, 90%, 100% correspond respectively to powers 8.7, 17.4, 26.1, 34.8, 43.5, 52.2, 60.9, 69.6, 78.3 and 87 mW.

For experiments with varying stimulation durations, we performed optogenetic stimulations of 20 ms, 50 ms, 100 ms, 200 ms, 500 ms, 1 s and 2 s, keeping in each case a period of 10 s (*i.e.* for the 20 ms stimulation for example, each period was composed of 9.98 s without stimulation and 20 ms of stimulation). Each recording was made up of 12 periods so that the total time was 120 s.

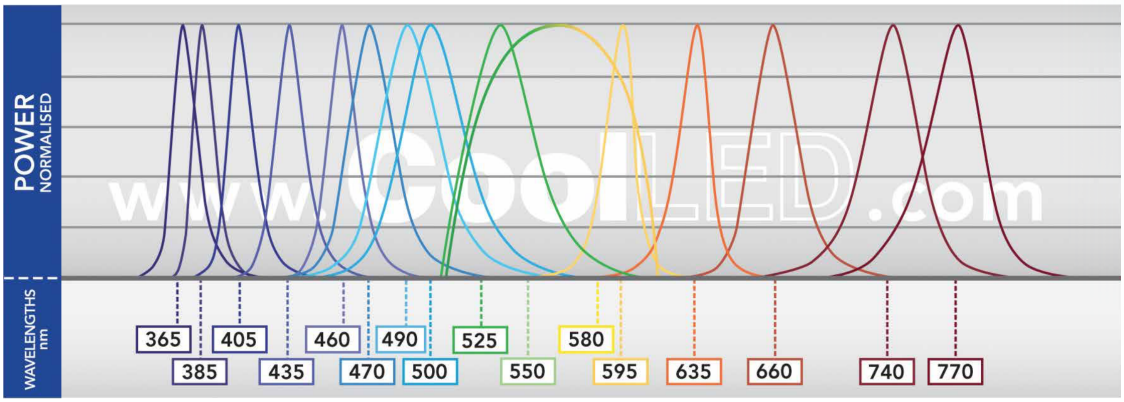

Figure 12: Excitation spectra of the Cool-LED pE-4000 used for optogenetic stimulations. We used a stimulation light at 490 nm wavelength (illustration taken from the Cool-LED pE-4000 user manual).

5.5 Fluorescence intensity spatial profiles

Spatial profiles were computed with the software Fiji, defining for each recording the same profile of 350 pixels in length passing through the stimulated region.

Supplementary Figures – Appendix

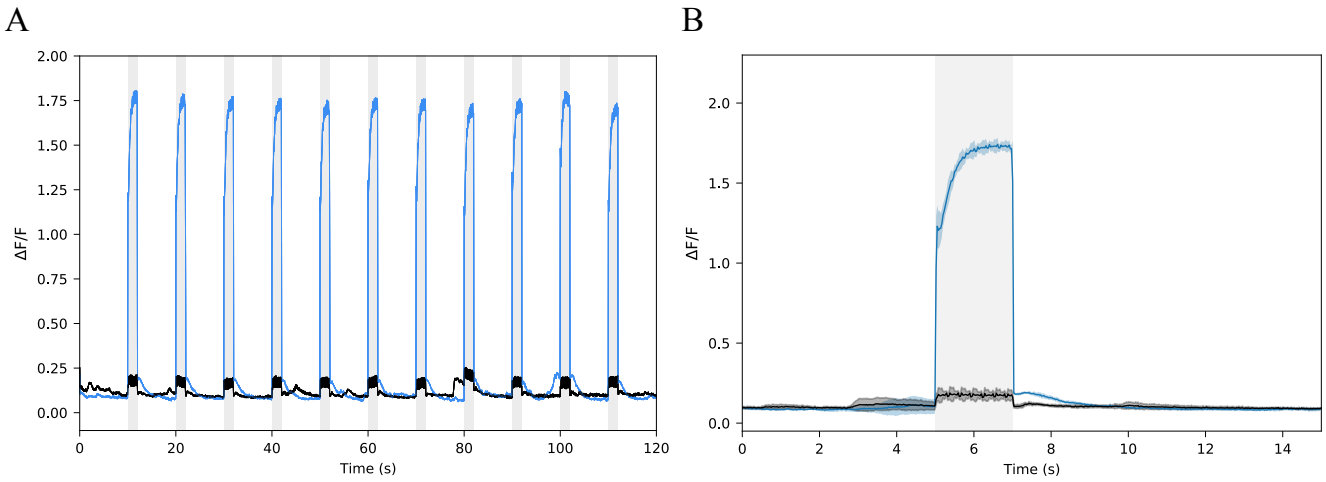

Figure 13: ΔF/F traces observed in control fish not expressing channelrhodopsin (jRGECO1b+ ; GFP-). **A.** Averaged ΔF/F trace observed for 2 s of stimulation at 100% of stimulation intensity. The blue trace corresponds to a stimulation in the optic tectum whereas the black trace corresponds to a stimulation outside of the brain. Traces were averaged over 10 neurons located in the stimulation region (optic tectum). **B.** ΔF/F trace of the panel A averaged over 10 trials The thick line represents the mean and shaded regions the standard deviation.

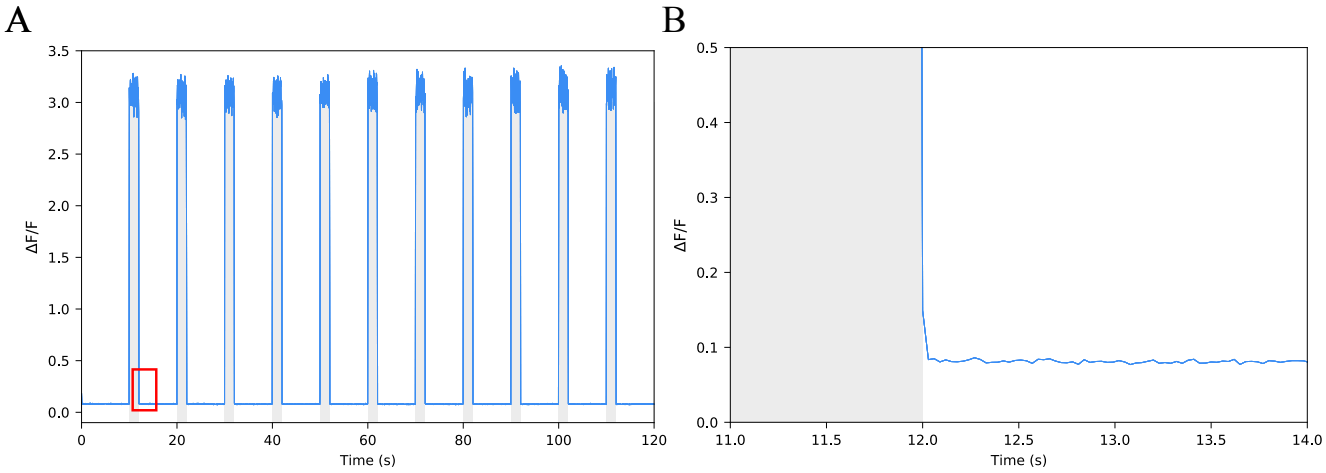

Figure 14: ΔF/F traces observed in control experiment on a red fluorescent marker (4-di-2asp) in agarose. **A.** Averaged ΔF/F trace observed for 2 s of stimulation at 100% of stimulation intensity. Traces were averaged over pixels in the stimulation region. **B.** Zoom on the red box in panel A. There is no fluorescence activity recorded just after the end of an optogenetic stimulation.

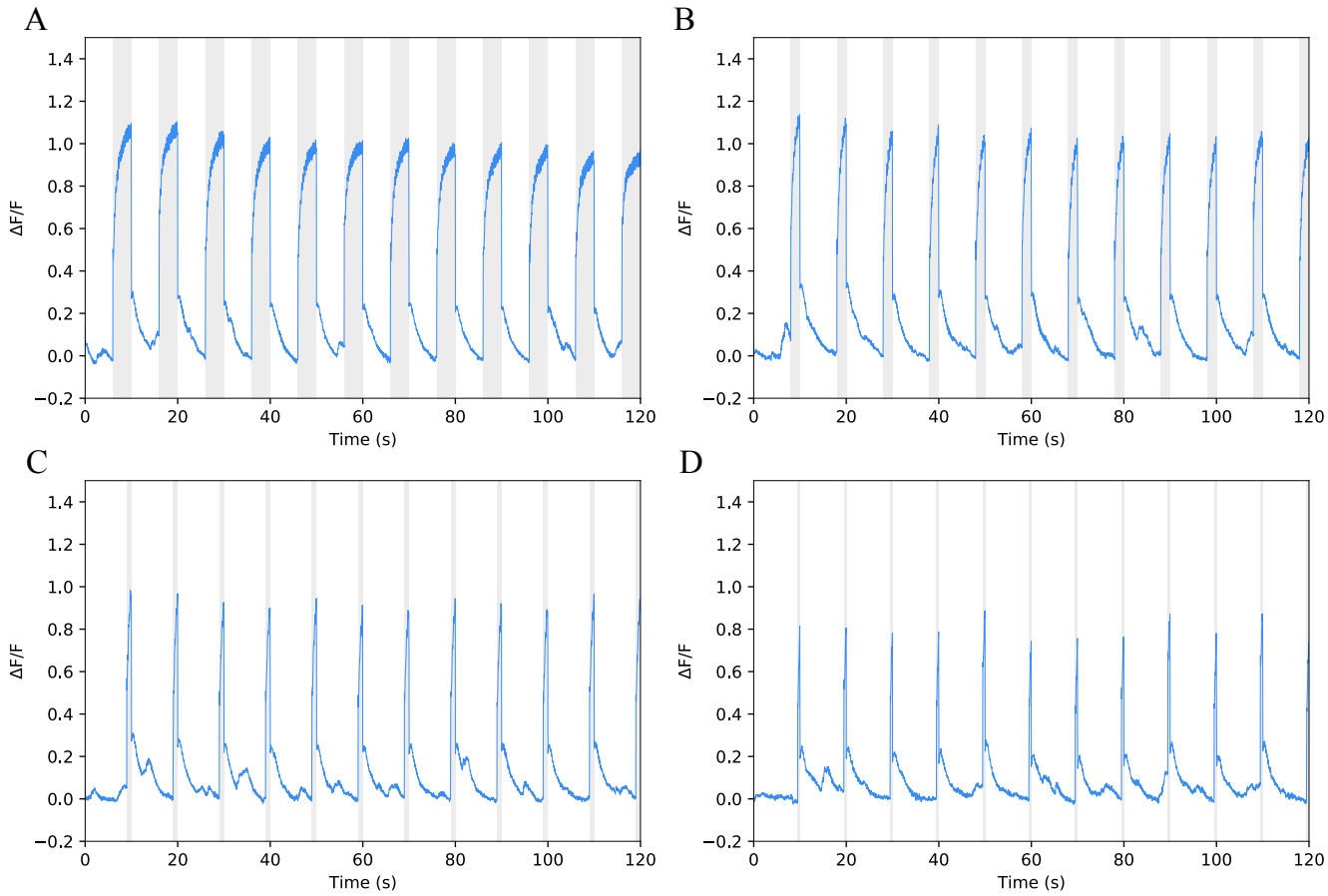

Figure 15: ΔF/F traces observed in the stimulation layer for different stimulation durations. Each trace is averaged over ten neurons located in the stimulation region (see stimulation mask, Figure 18A). **A.** Averaged ΔF/F trace observed for 4 s of stimulation at 100% of stimulation intensity. **B.** Averaged ΔF/F trace observed for 2 s of stimulation at 100% of stimulation intensity. **C.** Averaged ΔF/F trace observed for 1 s of stimulation at 100% of stimulation intensity. **D.** Averaged ΔF/F trace observed for 500 ms of stimulation at 100% of stimulation intensity.

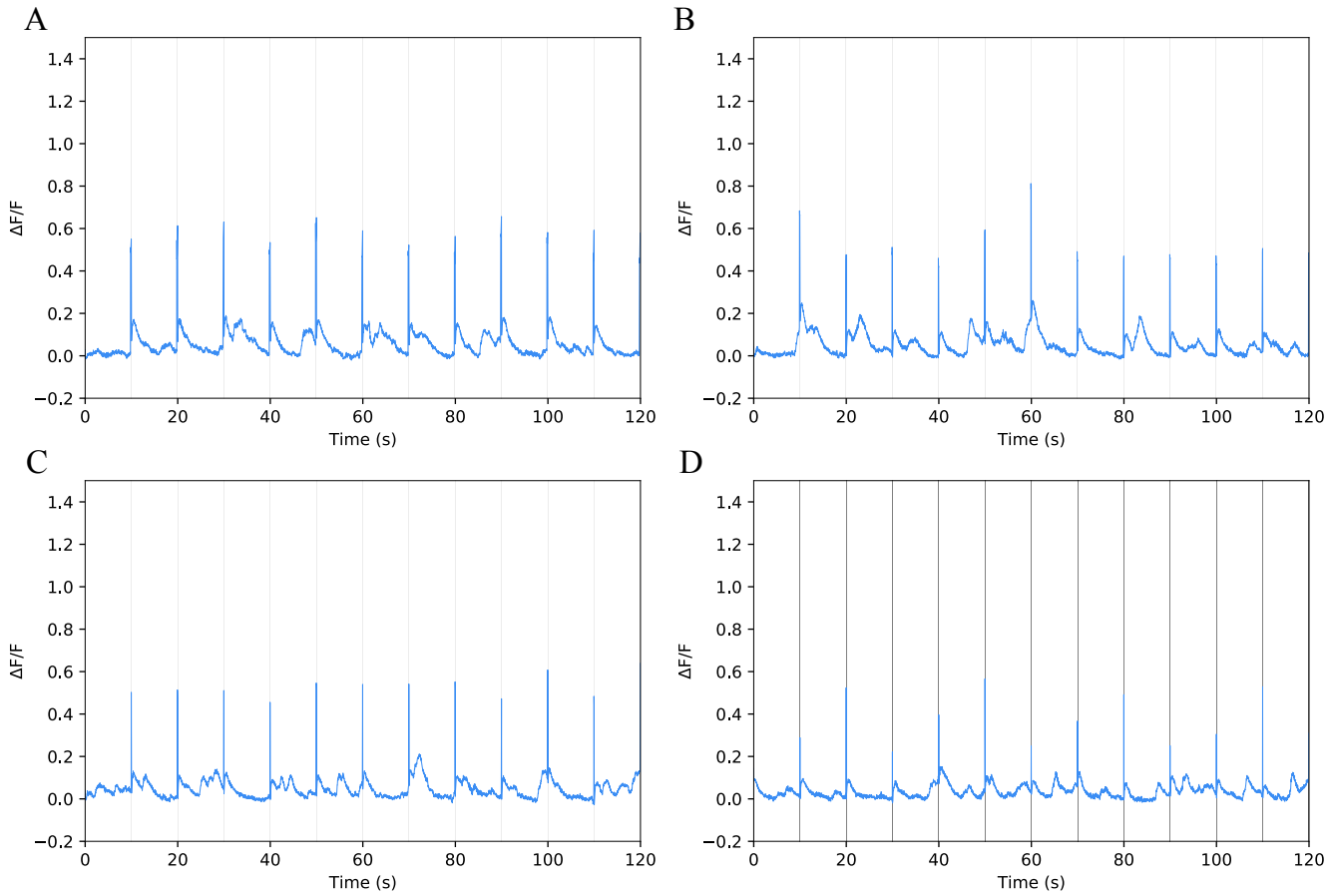

Figure 16: ΔF/F traces observed in the stimulation layer for different stimulation durations. Each trace is averaged over ten neurons located in the stimulation region (see stimulation mask, Figure 18A). **A.** Averaged ΔF/F trace observed for 200 ms of stimulation at 100% of stimulation intensity. **B.** Averaged ΔF/F trace observed for 100 ms of stimulation at 100% of stimulation intensity. **C.** Averaged ΔF/F trace observed for 50 ms of stimulation at 100% of stimulation intensity. **D.** Averaged ΔF/F trace observed for 20 ms of stimulation at 100% of stimulation intensity.

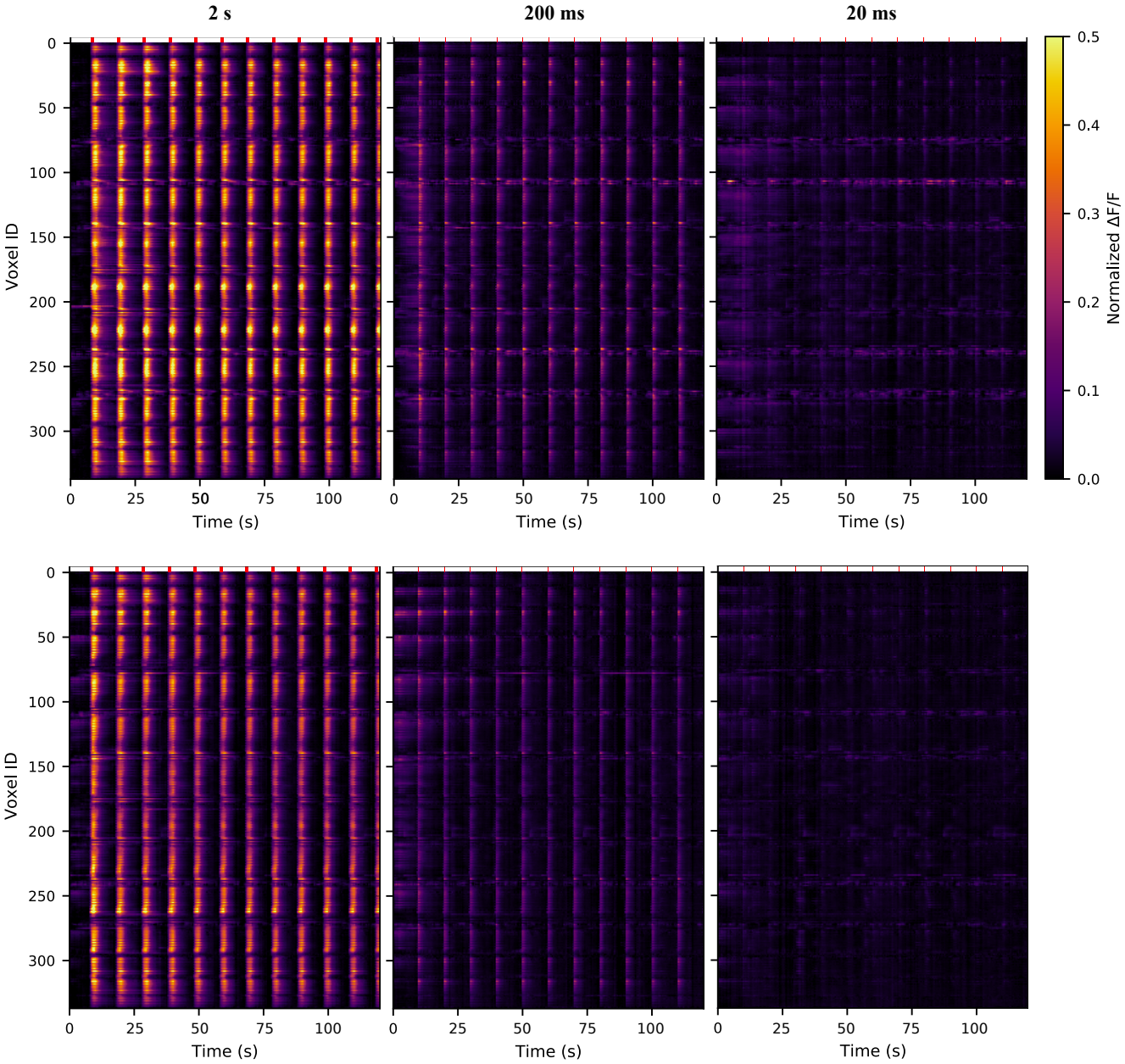

Figure 17: Comparison of voxel activities for two different optogenetic stimulation sites and three different stimulation durations. The upper panel represents the normalized ΔF/F over time for an optogenetic stimulation in the optic tectum (see stimulation mask, Figure 18A). The bottom panel represents the normalized ΔF/F over time for the same optogenetic stimulation in the cerebellum (see stimulation mask, Figure 18B). Red top ticks represent stimulation durations.

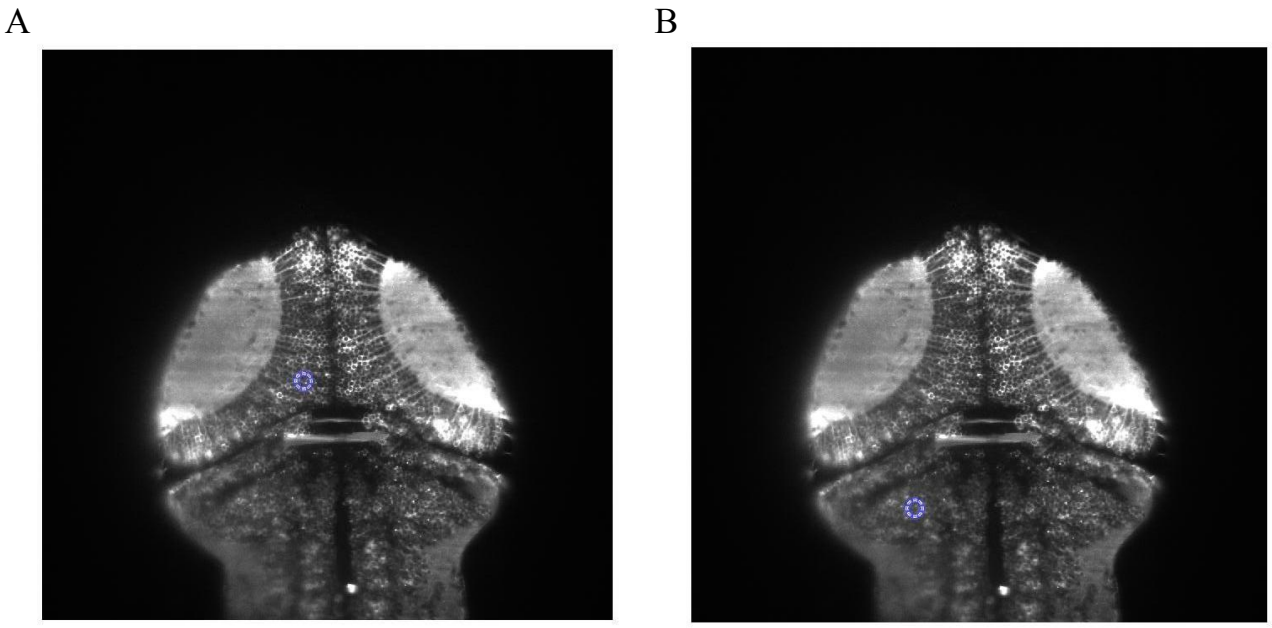

Figure 18: Masks used for optogenetic stimulations with different durations. **A.** Stimulation mask drawn in the optic tectum of a 5 dpf zebrafish larva. **B.** Stimulation mask drawn in the cerebellum of a 5 dpf zebrafish larva.

Bibliography

[1] A. Aldo Faisal, Luc P. J. Selen, and Daniel M. Wolpert. Noise in the nervous system. *Nature Reviews Neuroscience*, 9(4):292–303, April 2008.

[2] Peter Dayan and L. F. Abbott. *Theoretical neuroscience: computational and mathematical modeling of neural systems*. Computational neuroscience. MIT Press, Cambridge, Mass., first paperback ed edition, 2005. OCLC: 255027508.

[3] Kenneth D. Harris. Neural signatures of cell assembly organization. *Nature Reviews Neuroscience*, 6(5):399–407, May 2005.

[4] P. Berkes, G. Orban, M. Lengyel, and J. Fiser. Spontaneous Cortical Activity Reveals Hallmarks of an Optimal Internal Model of the Environment. *Science*, 331(6013):83–87, January 2011.

[5] John P Cunningham and Byron M Yu. Dimensionality reduction for large-scale neural recordings. *Nature Neuroscience*, 17(11):1500–1509, November 2014.

[6] G. E. Hinton. Reducing the Dimensionality of Data with Neural Networks. *Science*, 313(5786):504–507, July 2006.

[7] Simona Cocco, Rémi Monasson, Lorenzo Posani, and Gaia Tavoni. Functional networks from inverse modeling of neural population activity. *Current Opinion in Systems Biology*, 3:103–110, June 2017.

[8] Nikita Vladimirov, Chen Wang, Burkhard Höckendorf, Avinash Pujala, Masashi Tanimoto, Yu Mu, Chao-Tsung Yang, Jason D. Wittenbach, Jeremy Freeman, Stephan Preibisch, Minoru Koyama, Philipp J. Keller, and Misha B. Ahrens. Brain-wide circuit interrogation at the cellular level guided by online analysis of neuronal function. *Nature Methods*, 15(12):1117–1125, December 2018.

[9] Ofer Yizhar, Lief E. Fenno, Thomas J. Davidson, Murtaza Mogri, and Karl Deisseroth. Optogenetics in Neural Systems. *Neuron*, 71(1):9–34, July 2011.

[10] Or A. Shemesh, Dimitrii Tanese, Valeria Zampini, Changyang Linghu, Kiryl Piatkevich, Emiliano Ronzitti, Eirini Papagiakoumou, Edward S. Boyden, and Valentina Emiliani. Temporally precise single-cell-resolution optogenetics. *Nature Neuroscience*, 20(12):1796–1806, December 2017.

[11] Hod Dana, Boaz Mohar, Yi Sun, Sujatha Narayan, Andrew Gordus, Jeremy P Hasseman, Getahun Tsegaye, Graham T Holt, Amy Hu, Deepika Walpita, Ronak Patel, John J Macklin, Cornelia I Bargmann, Misha B Ahrens, Eric R Schreiter, Vivek Jayaraman, Loren L Looger, Karel Svoboda, and Douglas S Kim. Sensitive red protein calcium indicators for imaging neural activity. *eLife*, 5:e12727, March 2016.

[12] Thijs L. van der Plas, Jérôme Tubiana, Guillaume Le Goc, Geoffrey Migault, Volker Bormuth, Bernhard Englitz, and Georges Debrégeas. A maximum entropy graphical model unveils brain-wide neural assembly organization in zebrafish. not published.

[13] Geoffrey Migault, Thijs L. van der Plas, Hugo Trentesaux, Thomas Panier, Raphaël Candelier, Rémi Proville, Bernhard Englitz, Georges Debrégeas, and Volker Bormuth. Whole-Brain Calcium Imaging during Physiological Vestibular Stimulation in Larval Zebrafish. *Current Biology*, 28(23):3723–3735.e6, December 2018.